J Mater Sci (2018) 53:12132–12144

Composites

Effect of restricted geometry and external pressure on the phase transitions in ammonium hydrogen sulfate confined in a nanoporous glass matrix

Ekaterina A. Mikhaleva[1], Igor N. Flerov[1,2,*], Andrey V. Kartashev[1,3], Mikhail V. Gorev[1,2], Maxim S. Molokeev[1,2,4], Evgeniy V. Bogdanov[1,5], Vitaliy S. Bondarev[1,2], Leonid N. Korotkov[6], and Ewa Rysiakiewicz-Pasek[7]

[1] *Kirensky Institute of Physics, Federal Research Center KSC SB RAS, Akademgorodok, 50, Bld. 38, Krasnoyarsk, Russia 660036*
[2] *Siberian Federal University, Krasnoyarsk, Russia 660074*
[3] *Astafijev Krasnoyarsk State Pedagogical University, Krasnoyarsk, Russia 660049*
[4] *Department of Physics, Far Eastern State Transport University, Khabarovsk, Russia 680021*
[5] *Krasnoyarsk State Agrarian University, Krasnoyarsk, Russia 660049*
[6] *Voronezh State Technical University, Voronezh, Russia 394026*
[7] *Division of Experimental Physics, Faculty of Fundamental Problems of Technology, Wroclaw University of Science and Technology, 50-370 Wrocław, Poland*

Received: 29 January 2018
Accepted: 15 May 2018
Published online: 29 May 2018

ABSTRACT

A study of heat capacity, thermal dilatation, susceptibility to hydrostatic pressure, permittivity and polarization loops was carried out on NH_4HSO_4–porous glass nanocomposites (AHS + PG) as well as empty glass matrices. The formation of dendrite clusters of AHS with a size, d_{cryst}, exceeding the pore size was found. An insignificant anisotropy of thermal expansion of AHS + PG showing statistically uniform distribution of AHS with random orientations of nanocrystallites over the matrix was observed. The effect of internal and external pressures on thermal properties and permittivity was studied. At the phase transition $P\text{-}1 \leftrightarrow Pc$, a strongly nonlinear decrease in the entropy ΔS_2 and volume strain $(\Delta V/V)_{T2}$ was observed with decreasing d_{cryst}. The linear change in temperatures of both phase transitions $P\text{-}1 \leftrightarrow Pc \leftrightarrow P2_1/c$ under hydrostatic pressure is accompanied by the expansion of the temperature range of existence of the ferroelectric phase Pc, while this interval narrows as d_{cryst} decreases.

Address correspondence to E-mail: flerov@iph.krasn.ru

https://doi.org/10.1007/s10853-018-2467-1

Introduction

Despite the wide popularity of porous glasses due to the possibility of their use in various scientific studies and many industrial applications, there is a series of questions and problems related to their preparation, certification and, especially, application [1–3]. Recently, a special attention was paid to the porous glasses as a basis for creating composite materials. A lot of publications appeared describing the researches of glass matrices with embedded materials of various natures [4–9], in particular multiferroics [4, 6, 7] and/or ferroelectrics [10–19]. In the latter case, the main direction of research of glass composites was, as a rule, associated with the study of behavior of the dielectric properties of the ferroelectric component in confined geometry and its dependence on a type of the matrices and diameter of the pores [10, 11, 13, 15–19]. Other properties, in particular thermodynamic, have been examined to a lesser extent. At the same time, the study of the heat capacity and thermal dilatation of composites provides information on the effect of interaction between components of composites on entropy and deformation associated with the ferroelectric phase transitions [17, 20–23]. The effect of external pressure on the ferroelectric nanocomposites has not been examined at all. Recently, it has been shown that high pressure is a very powerful tool to modify nanostructured materials, study interactions at the nanoscale and design new nanomaterials [24]. In this connection, the data on the heat capacity and thermal dilatation of the nanoporous matrices are also very important. However, as far as we know, thermodynamic properties of porous glasses were not studied systematically.

This paper presents the results of studies of nanocomposites prepared on the basis of ammonium hydrogen sulfate, NH_4HSO_4, embedded into borosilicate glass matrices. We intended to analyze the effect of internal pressure associated with the confined geometry as well as hydrostatic pressure on the entropy, elastic strain and baric coefficients of the phase transitions in ferroelectric component. For this purpose, the heat capacity, thermal dilatation, susceptibility to external hydrostatic pressure and dielectric properties of the nanocomposites were investigated. To be correct when analyzing data on the properties of ferroelectric component, heat capacity and thermal expansion of the nanoporous glasses were also studied. The originality of our investigations compared to recent studies [17, 21, 23] of heat capacity and permittivity of nanocomposites with NH_4HSO_4 is associated with the following points:

1. the porous glasses were filled with molten NH_4HSO_4 to reliably avoid the presence of an aqueous solution in the pores;
2. studies of the heat capacity were performed using an adiabatic calorimeter showing high resolution and high stability of measurements instead of the low sensitive differential scanning calorimeter [23];
3. permittivity was studied at atmospheric and high pressures;
4. investigations of thermal dilatation and the effect of pressure on phase transitions are pioneering;
5. detailed studies of the thermodynamic properties of porous borosilicate glasses were carried out.

The choice of the object of research is due to several reasons. First, NH_4HSO_4 undergoes a succession of the phase transitions $P\text{-}1(P1)$ (T_2 = 160 K) $\leftrightarrow$ Pc (T_1 = 271.7 K) $\leftrightarrow$ $P2_1/c$ of the first and second order, respectively [24–27]. (Two possible space groups for the phase at $T < T_2$ are presented, since there is still no consensus on the nature of the corresponding structural transformation.) Second, previously we have carried out studies of the effect of chemical pressure on phase transitions, as well as electro- and barocaloric effects in solid solutions $(NH_4)_{1-x}Rb_xHSO_4$ [28]. Third, in the manufacture of composites, we used an important advantage of NH_4HSO_4, in comparison with other water-soluble ferroelectrics, associated with the possibility of its melting without decomposition. Recent comparative studies of the NH_4HSO_4 samples prepared from an aqueous solution and the melt have shown quite similar thermodynamic and dielectric properties [29].

Sample preparation and measurement technique

Hereinafter, NH_4HSO_4, borosilicate porous glasses and NH_4HSO_4–glass nanocomposites will be labeled as AHS, PG and AHS + PG, respectively. For the present study, we have used PGs with five different pore sizes. The samples of the glass matrices with

average diameter of pores 5, 23, 46, 160 and 320 nm were cut out in the form of flat plates of about $1.0 \times 1.0 \times 0.05$ cm^3. The porosity was determined by the relative mass decrement method during the preparation of the samples as well as evaluated by adsorption of a water stream and a mercury intrusion porosimetry. The pore sizes were determined in the framework of a cylindrical pore model. The methods of certification of samples studied one can also see in [1]. The porosity of different PGs was found in the range of 40–55% (Table 1).

The nanocomposites AHS + PG were fabricated by the immersion of empty PG into the melted AHS for several hours. To avoid the nonequilibrium state in AHS observed by Kosova et al. [30], subsequent cooling down to room temperature was carried out at a very low rate ($\sim$ 0.1 K min^{-1}). A mechanical polishing was used to remove microcrystals from the surfaces of the composite samples. The filling factor was estimated as the ratio of the volumes of the embedded AHS to the pores volume (Table 1). For dielectric measurements, silver electrodes were painted onto the samples' surfaces.

Characterization of AHS, PG and AHS + PG was carried out at room temperature by XRD using a Bruker D8 ADVANCE powder diffractometer (Cu-Kα radiation). Figure 1a depicts a diffraction pattern of PG46, which is typical for the other samples of PG and for the amorphous materials without any crystalline phases. The results of Rietveld refinement for the samples AHS and AHS + PG46 are shown in Fig. 1b, c. No additional phases were observed in ammonium hydrogen sulfate as well as in all the nanocomposites. The information on the ferroelectric nanoparticles size, d_{cryst}, filling the pores of matrix was obtained using TOPAS 4.2 program [31]. The

Table 1 Characteristics of porous glasses and nanocomposites

Glasses		Nanocomposites	
d_{pore} (nm)	Porosity (%)	Filling factor (%)	d_{cryst} (nm)
5	42	38	9.0 (4)
23	55	90	70 (2)
46	55	67	47 (2)
160	46	81	500 (39)
320	50	74	115 (15)

d_{pore} and d_{cryst} are the sizes of pores and nanoparticles, respectively

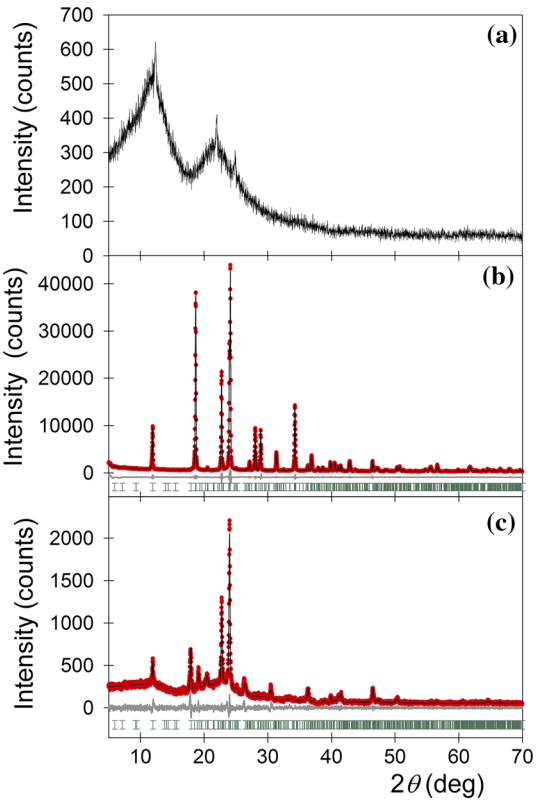

Figure 1 XRD patterns: **a** empty PG46; **b** AHS; **c** AHS + PG46.

high reliability of the obtained data is confirmed by relatively small values of estimated standard deviation presented in Table 1 which shows that an increase in the pore diameter is not accompanied by monotonic increase in d_{cryst}. Moreover, in the case of three composites with PG5, PG23 and PG160, d_{cryst} exceeds the pore diameter. Recently, similar situation observed in nanocomposites with the embedded $NaNO_2$ was explained as associated with the formation of the dendrite clusters in pores [12].

The micromorphology of the surface of empty glasses and nanocomposites was examined using scanning electron microscopes (SEM) Hitachi TM3000 and Hitachi S-5500 (Hitachi High-Technologies Co., Ltd., Tokyo, Japan). The typical SEM images of the samples PG5, PG46 and AHS + PG46 are shown in Fig. 2. One can see noticeable loss of the image contrast in nanocomposites. Less distinct boundaries between the matrix material and the embedded ferroelectric AHS in comparison with the boundaries between the pores and the matrix body prove that pores of glass are filled by AHS to a substantial degree. Such a phenomenon was also

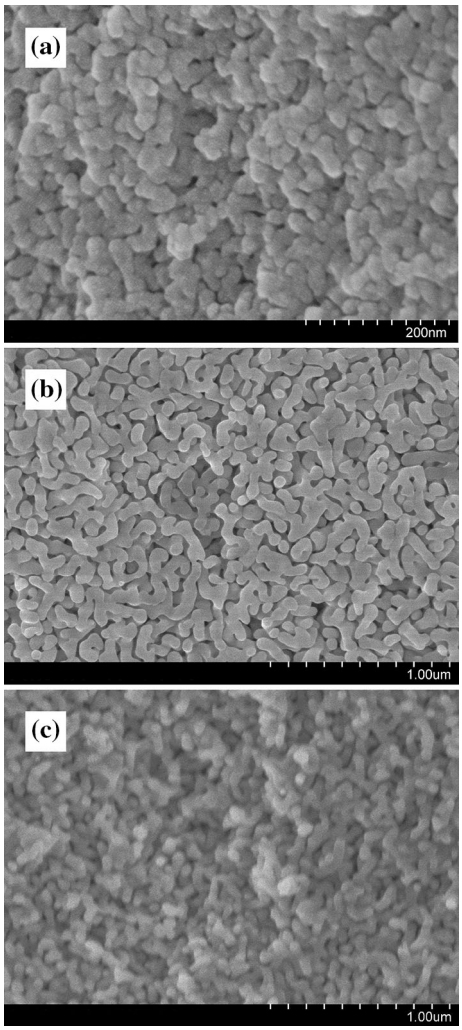

Figure 2 SEM images: **a** PG5; **b** PG46; **c** AHS + PG46.

observed earlier for example for nanocomposites $NaNO_2$ + PG [32].

In order to perform a correct analysis of the properties of AHS nanosized crystals embedded into the glass matrix, it is necessary to have information on the properties of glass matrices and AHS. Recently, we have studied thermodynamic properties of bulk AHS prepared from an aqueous solution and the melt and found that parameters characterizing both phase transitions are close to each other for the both samples [29]. To our knowledge, the data on thermodynamic properties of boron-silicate glasses are absent. So first of all we studied the heat capacity and thermal dilatation of PGs which were then filled with AHS.

Measurements of thermal expansion were performed using a push-rod dilatometer (NETZSCH model DIL-402C) with a fused silica sample holder. Experiments were carried out in the temperature range 100–300 K with a heating rate of 3 K min^{-1} in a dry He flux. The results were calibrated, by taking quartz as the standard reference, to remove the influence of system thermal expansion. Because of a large difference in thermal dilatation of PG and AHS, the uncertainty in measurements was individual, about 20% for PG and 8% for AHS + PG. However, the reproducibility of data obtained in successive series of all the measurements was not less than 5%.

Measurements of the heat capacity of samples examined in dilatometric experiments were taken in a wide temperature range of 82–300 K by means of a homemade adiabatic calorimeter with three screens, as described by Kartashev et al. [33]. The inaccuracy in the heat capacity determination did not exceed 0.5–1.0%. The heat capacity of the "sample + heater + contact grease" system was measured using discrete as well as continuous heating. In the former case, the calorimetric step was varied from 1.5 to 3.0 K. In the latter case, the system was heated at rates of $dT/dt \approx 0.15$–0.30 K min^{-1}. The heat capacities of the heater and contact grease were determined in individual experiments.

Dielectric properties were also studied in an adiabatic calorimeter. The temperature behavior of the permittivity ε was investigated using an E7-20 immittance meter at frequencies from 1 Hz up to 10^6 Hz while heating at a rate of about 0.5 K min^{-1}. The dielectric hysteresis (P–E loop) was examined using an aixACCT EASY CHECK 300 technique. The driving-field profile was a triangular wave of amplitude E_{max} = 5 kV cm^{-1}. The frequency of the measuring electric field was 250 Hz. Measurements of $\varepsilon(T)$ were taken only on nanocomposites because similar investigations on AHS [29] and empty PG [17] were carried out recently. In the latter case, it was shown that permittivity of PG does not depend significantly on temperature (in the range 120–400 K) and frequency at least up to $f = 10^6$ Hz.

The effect of hydrostatic pressure on the phase transitions in AHS component embedded in PG was studied using a piston-cylinder-type vessel associated with a pressure multiplier. Pressure of up to 0.25 GPa was generated using pentane as the pressure-transmitting medium. The inaccuracy in the measurements of pressure and temperature using a manganin gauge and a copper-constantan

thermocouple was about $\pm 10^{-3}$ GPa and $\pm$ 0.3 K, respectively.

The dependences $T_1(p)$ and $T_2(p)$ were studied by measuring both permittivity and the differential thermal analysis (DTA) signal. In the former case, the measurements were taken using the technique used in the studies at atmospheric pressure and described above. In the latter case, a germanium–copper thermocouple characterized by high sensitivity to change in temperature ($\sim$ 400 μV K^{-1}) was used [34]. Two junctions of the thermocouple were formed by soldering a copper wire 0.08 mm in diameter to a germanium bar of 0.5 × 2.0 × 5.0 mm^3 dimensions. A sample of 0.5 × 4.0 × 4.0 mm^3 dimensions was glued onto one of the two junctions of a thermocouple. A quartz sample cemented to the other junction was used as a reference substance. To ensure the reliability of the results, the measurements under both increasing and decreasing pressure cycles were performed.

Results and discussion

Figure 3a depicts the temperature dependences of the specific heat, $C_p(T)$, of PGs. Difference in the chemical composition of the borosilicate glasses studied is not significant, and as a result, one can see a rather good agreement between the data for the samples with average diameter of porous 5, 46 and 320 nm in the whole temperature range examined, 100–300 K. The maximum difference between curves $C_p(T)$ observed at about 100 K does not exceed several percents.

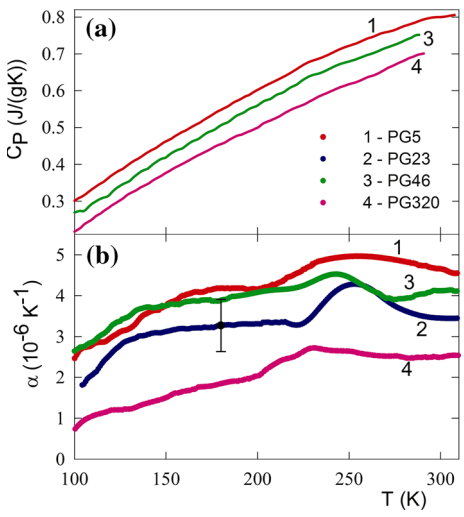

Figure 3 Temperature dependences of: **a** the specific heat (curves 3 and 4 are shifted down at 0.05 and 0.10 J g^{-1} K^{-1}, respectively); **b** the coefficient of linear thermal expansion of PGs.

In contrast to the specific heat, thermal dilatation of PGs was found dependent on the pore size (Fig. 3b). The largest and smallest values of the coefficient of linear thermal expansion, α, are characteristic for PG5 and PG320, respectively, and differ from each other almost in two times. However, taking into account very small α value of PGs and as a result increased inaccuracy in their determination, one can think that the difference observed is not so large.

All the $\alpha(T)$ dependences of PGs demonstrate a bump in rather wide temperature range $\sim$ 220–290 K. We think that it can be associated with a small amount of water left in the pores because of ambient pressure of the α measurements. Due to a high vacuum ($\sim 10^{-6}$ mm Hg) in experimental chamber of the adiabatic calorimeter, no anomalies on the $C_p(T)$ dependences of PGs were observed (Fig. 3a).

Experimental data obtained by adiabatic calorimeter for AHS + PG nanocomposites are shown in Fig. 4a. The temperature dependences of the heat capacity demonstrate pronounced anomalies associated with the phase transition $P\text{-}1 \leftrightarrow Pc$ at T_2. Due to small heat capacity change at T_1 even in pure molten AHS [29], the anomalies of $C_p(T)$ in nanocomposites in the region of the $Pc \leftrightarrow P2_1/c$ transformation are decreased and smeared.

To obtain information on the phase transition entropies, the anomalous contribution, ΔC_p, to the total heat capacity C_p was extracted. This procedure was carried out using a polynomial functions describing nonanomalous heat capacity of the nanocomposites consisted of lattice heat capacity of AHS and $C_p(T)$ of PG, $C_{reg} = C_L + C_{PG}$. For this aim, the experimental data $C_p(T)$ of AHS + PG were taken far from the transition points in AHS component ($T < 145$ K and $T > 273$ K) as it was done during the analysis of the heat capacity of bulk AHS [29]. In all the cases, the average deviation of the experimental data from the smoothed curves does not exceed 1.5%. The regular contributions into the total heat capacities of the nanocomposites are shown as a dashed line in Fig. 4a. One can see that the degree of the smearing as well as decreasing both anomalies changes with the pore size change.

The total excess entropy $\Sigma\Delta S = \Delta S_1 + \Delta S_2$ associated with the successive phase transitions $P\text{-}1 \leftrightarrow Pc \leftrightarrow P2_1/c$ was determined by integrating the

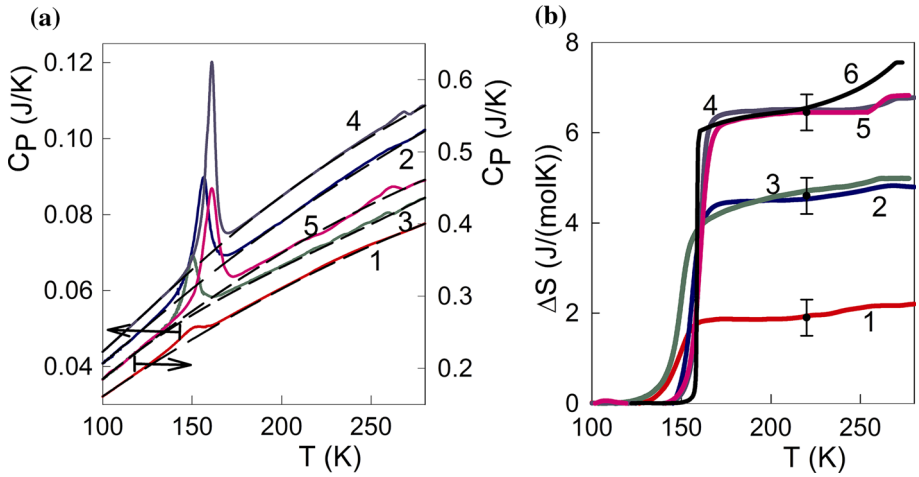

Figure 4 **a** Temperature dependences of the heat capacity of the nanocomposites. The dashed lines are the regular heat capacities. **b** Behavior of the excess entropy associated with the $P\text{-}1 \leftrightarrow Pc \leftrightarrow P2_1/c$ phase transitions in AHS component. 1—AHS + PG5, 2—AHS + PG23, 3—AHS + PG46, 4—AHS + PG160, 5—AHS + PG320, 6—AHS.

area below the $\Delta C_p/T$ versus T curves taking into account the mass of AHS in each of the nanocomposites. Figure 4b shows the temperature behavior of $\Sigma\Delta S$ in AHS confined in PGs. There is a significant decrease in $\Sigma\Delta S$ values with decrease in pore size or nanoparticle size. This suggests a decrease in the disordering of structural elements in the initial phase $P2_1/c$ of AHS confined in glass matrix. In addition, a strong smearing of the change in entropy at T_1 and T_2 was also observed which can be associated with heterogeneity of the sizes of pores as well as crystallites.

Linear thermal expansion coefficient $\alpha \approx (27\text{–}70) \times 10^{-6}\ K^{-1}$ of AHS in the temperature ranges far from the phase transition points [26, 29, 35] is many times as much compared to $\alpha \approx (1\text{–}5) \times 10^{-6}\ K^{-1}$ of empty PGs (Fig. 3b). A large difference in α of the matrix and AHS can lead to an increase of α of AHS + PG compared to PGs and to the appearance of intrinsic elastic stress which will change at temperature variation. However, because PGs were filled with AHS at about 430 K, further cooling down to room temperature and below should be accompanied by more rapid decrease in the volume of AHS compared to PG and, as a result, tensile stresses can appear in the elastic interactions between two components which will increase upon cooling and decrease upon heating.

The results of dilatometric measurements on nanocomposites are presented in Fig. 5. In the temperature regions of nonanomalous behavior of the thermal expansion, one can see a distinct difference between the α values for the different AHS + PG samples (Fig. 5a) which is due to the different filling factor, the nanoparticle size (Table 1) and, to a lesser

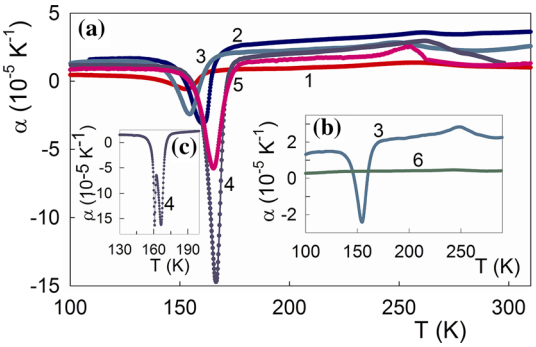

Figure 5 **a** Temperature dependences of the thermal expansion coefficient of the nanocomposites; 1—AHS + PG5, 2—AHS + PG23, 3—AHS + PG46, 4—AHS + PG160, 5—AHS + PG320, 6—PG46. **b** Comparison of α for AHS + PG46 and PG46. **c** Thermal dilatation around T_2 in the AHS + PG160 sample with part of the melt on its surface.

extent, the difference in the α values of PGs (Fig. 3b). Indeed, the filling factor is, for example, about 38 and 90% for AHS + PG5 and AHS + PG23, respectively, and this determines the smallest ($2.5 \times 10^{-6}\ K^{-1}$) and largest ($36 \times 10^{-6}\ K^{-1}$) values of α at 300 K.

The anomaly of thermal expansion of composites is determined by many factors, such as pore and crystallite sizes, mass of ferroelectric components, filling factor. We believe that the strongest and narrowest $\alpha(T)$ anomaly in the composite AHS + PG160 is due to the fact that this composite has the largest crystallite size (Table 1) and, as a result, is closer to bulk AHS. At the same time, the temperature of the phase transition and the anomalous volume deformation recalculated into volume strain $(\Delta V/V)_{T2}$ associated with the actual volume V of AHS in each sample (Fig. 6c) within the error of its determination fit into

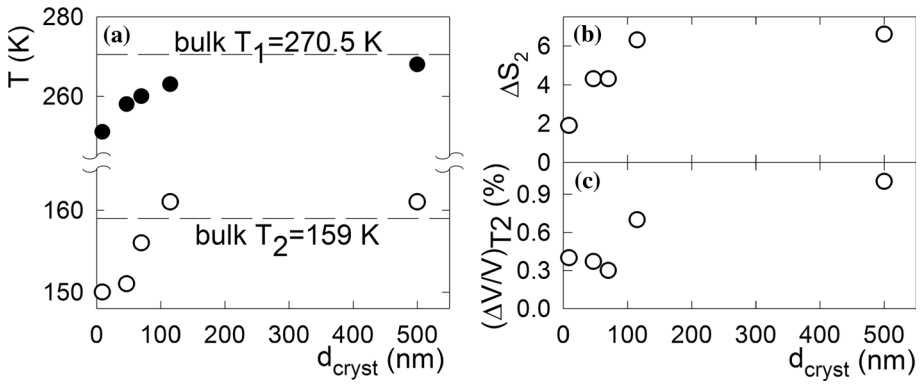

Figure 6 Effect of the nanoparticle size of AHS on **a** phase transition temperatures in nanocomposites AHS + PG and the change in **b** entropy ΔS_2 (J mol^{-1} K^{-1}) and **c** volume strain $(\Delta V/V)_{T2}$ at the $P\text{-}1 \leftrightarrow Pc$ transformation.

the general relationships of the thermal parameters at the decrease in d_{cryst} (Fig. 6a–c).

Figure 5b demonstrates the $\alpha(T)$ dependences of PG320 and AHS + PG320 revealing that a linear coefficient of the thermal expansion of the AHS + PG samples is several times greater than α of PG. These data are given by way of example, but are true for all the nanocomposites studied. Such an effect of AHS on the thermal expansion of nanocomposites can be associated only with a strong elastic interaction between the ferroelectric and the glass components.

Nanocomposites under study consist of an isotropic glass matrix and a crystalline ferroelectric with monoclinic symmetry in initial room temperature phase. To check the effect of an anisotropic component on the thermal expansion of a composite based on an isotropic matrix, we performed measurements of α in three directions on AHS + PG320: along two sides of the plate and perpendicular to its largest surface. The difference in α for different directions did not exceed 10–15%. Taking into account the inaccuracy of dilatometric measurements, the distribution of AHS over the volume of the nanocomposites can be considered as statistically uniform with equiprobable orientations of crystalline nanoparticles in all directions.

One of the features of the nanocomposites studied is that the temperatures, T_1 and T_2, of phase transitions are characterized by a nonmonotonic change with decreasing pore size. Figure 6a depicts dependences of the both phase transition temperatures on the size of nanoparticles in comparison with the values for bulk AHS [29]. A reduction of d_{cryst} from 500 nm down to 9 nm is accompanied by narrowing of the temperature region of ferroelectric Pc phase existence.

The behavior of the temperatures of phase transitions in nanocomposites demonstrates very interesting general and specific features. At $d_{cryst} \leq 100$ nm, T_1 and T_2 strongly decrease with decreasing nanoparticle size. In all nanocomposites, the temperature of the phase transition $Pc \leftrightarrow P2_1/c$ is lower than T_1 in the bulk AHS. At that time, T_2 in AHS + PG160 and AHS + PG320 exceeds the bulk value (Fig. 6a). To verify the latter effect, we left part of the AHS melt on the surface of the AHS + PG160 sample and performed measurements of $\alpha(T)$. Figure 5c demonstrates two peaks on the $\alpha(T)$ curve associated with the $P\text{-}1 \leftrightarrow Pc$ phase transition in the AHS component and the bulk AHS on the surface of the sample. Thus, there really is a difference in the values of T_2 in the "free" and confined AHS. Below we return to discussing the features above in the behavior of T_1 and T_2 in comparison with the effect of hydrostatic pressure.

Experimental data on $\alpha = L^{-1} \times (\Delta L/\Delta T)$ are presented in Fig. 5a for a number of nanocomposites, where L is the linear dimension of the glass matrix plate. To obtain information on the change in the volume strain at the first-order transition $P\text{-}1 \leftrightarrow Pc$ in the AHS component, we recalculated α into volume strain $(\Delta V/V)_{T2}$ taking into account the actual volume V of AHS in each sample. Figure 6b, c shows dependences of entropy ΔS_2 and volume strain $(\Delta V/V)_{T2}$ on the nanoparticle size. It can be seen that at $d_{cryst} \leq 100$ nm, both values greatly decrease, just as it was found above for the temperatures T_1 and T_2. A rather large difference in the change in the volume strain at T_2 in AHS ($\sim$ 1.5%) and in composites even with rather large-sized particles ($\sim$ 1.0% in AHS + PG160) suggests that the glass matrix prevents the expansion of the ferroelectric component. This is also confirmed by the large difference in the values of α of

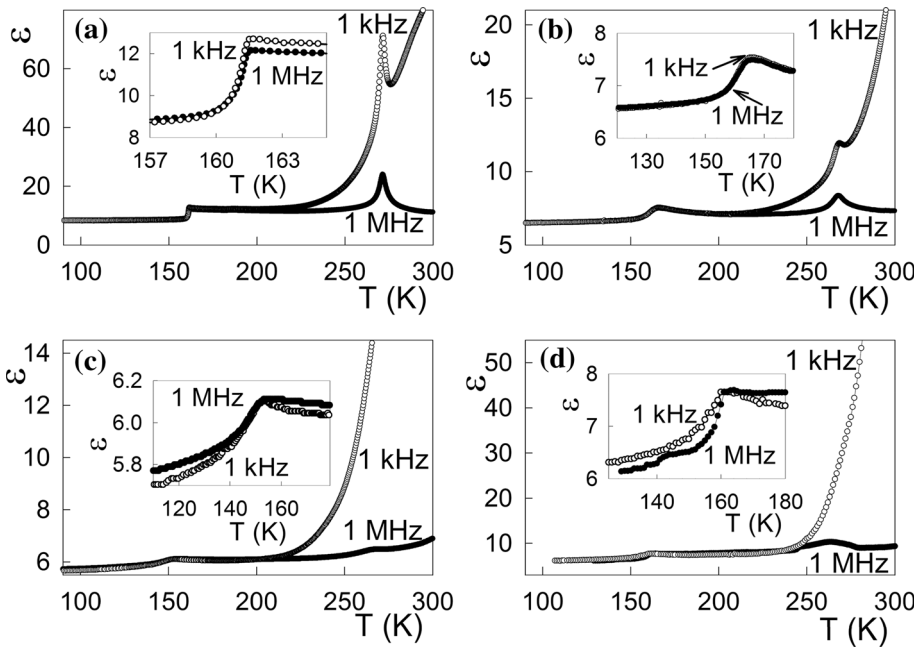

Figure 7 Temperature dependences of permittivity at different f for **a** bulk AHS, **b** AHS + PG320, **c** AHS + PG46, **d** AHS + PG23. Insets show the permittivity behavior near T_2.

glass matrices (Fig. 3), nanocomposites (Fig. 5) and bulk AHS [29] in temperature regions far from the phase transition points.

The temperature dependence of the permittivity of some nanocomposites in comparison with $\varepsilon(T)$ of bulk AHS [29] is shown in Fig. 7. The $\varepsilon(T)$ curves for all samples show specific features characteristic of phase transitions of the first and second order: jump at T_2 and more or less pronounced peak at T_1. At a frequency of $f < 1$ kHz, a strong increase in ε was observed at $T > 200$ K, which decreased with increasing f to 1 MHz. The increase in the low-frequency permittivity in the nanocomposites with AHS and its strong frequency dependence were also observed in [17, 18] and assumed to be associated with the high proton mobility and the appearance of space charge polarization [18].

The temperatures of both phase transitions in all investigated nanocomposites are independent of frequency variation and agree well with those found in calorimetric measurements.

The values of both the stepwise change in ε at T_2 and the ε peak at T_1 were changed in irregular manner with decreasing pore size, which can be due to both the different filling factor of nanocomposites and the particle size (Table 1). In spite of the smeared ε anomalies in AHS + PG, the peak-like and stepwise behavior of permittivity at T_1 and T_2, respectively, at different frequencies as well as the data on the heat capacity, entropy and thermal expansion proves that

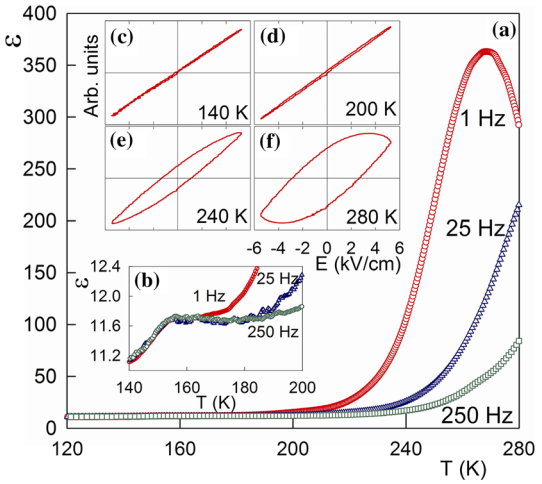

Figure 8 **a**, **b** Dependence of permittivity on temperature for AHS + PG46 at different frequencies; **c**–**f** dielectric hysteresis loops at the corresponding temperatures.

the order of both transformations is kept in all the nanocomposites studied.

Similar to studies on bulk ceramic AHS [29], we were not successful in examining the P–E loops in the composite AHS + PG46 (Fig. 8). Linear dependence of polarization versus electric field below T_2 is in accordance with the absence of spontaneous macroscopic polarization in the AHS single crystal [25, 26]. However, almost the same behavior $P(E)$ characteristic for nonpolar dielectrics was observed even at 200 K (Fig. 8d), i.e., far above T_2. The shape of the

loop appeared at 240 K is distorted and not characteristic for the classic ferroelectric material (Fig. 8e). In this case, the determination of the actual value of the polarization is impossible. Moreover, above T_1, in paraelectric phase, the shape of the loops is typical for the dielectrics with large losses (Fig. 8f) [36] which are also confirmed by strong dependence of the permittivity on frequency of E (Figs. 7 and 8a). The most probable cause of this phenomenon is associated with high electrical conductivity, which was observed even in AHS single crystal [37]. It is interesting to compare the behavior of $P(E, T)$ in AHS + PG46 with the same in single-crystal AHS under hydrostatic pressure studied around T_2 [38]. Examination of the P–E loops was successful only upon cooling. Upon heating from phase P-1, they were not able to determine correctly T_2 even at low pressure due to a very long time of relaxation of the polarization: The equilibrium polar state was established after many hours.

Due to the specific features of the experimental installation, we were able to measure $P(E, T)$ only in the heating mode and, as a result, met the same difficulties. It should be noted that other properties (heat capacity, thermal dilatation, permittivity) showed that the structural transformation P-1–Pc occurred at T_2. In this way, we can assume the effects of restricted geometry (internal pressure in nanocomposites) and hydrostatic pressure on the behavior of polarization in nanocomposites and bulk crystal, respectively, as similar phenomena.

The hydrostatic pressure effect on the successive phase transitions $P2_1/c \leftrightarrow Pc \leftrightarrow P$-1 in AHS and AHS + PG320 was studied by the DTA and permittivity measurements.

The permittivity of both samples measured at a frequency $f = 1$ kHz and different pressures is presented in Fig. 9. Comparison of these data with those shown in Fig. 7 indicates a strong smearing of the ε anomaly associated with the second-order transformation $P2_1/c \leftrightarrow Pc$ in AHS + PG320.

Nevertheless, one can see that the increase in pressure results in a positive shift of T_1 in composite like bulk AHS. At the same time, T_2 decreases under external pressure in both samples. One can assume that the difference in the susceptibility of both temperatures to hydrostatic pressure is associated with different mechanisms of the phase transitions in AHS at T_1 and T_2 [37, 39–41].

The results of the DTA measurements under pressure on bulk AHS and AHS + PG320 in the region of the P-1 $\leftrightarrow$ Pc phase transition are shown in Fig. 10a, b.

The increase in pressure is accompanied by a significant reduction of the area under the DTA-signal peaks which is proportional to the entropy change ΔS_2 associated with the phase transition at T_2. The dependences $\Delta S_2(p)$ can be considered as linear with very close values of the coefficient $d\Delta S_2/dp = 30$ and 35 J mol^{-1} K^{-1} GPa^{-1} for AHS and AHS + PG320, respectively. Such a behavior of $\Delta S_2(p)$ correlates with decrease of ΔS_2 at the particle size reduction found in calorimetric experiments on the nanocomposites (Fig. 6b). Linear and strong nonlinear dependences $\Delta S_2(p)$ and $\Delta S_2(d_{cryst})$ show that decrease in the nanoparticle size is accompanied by strong nonlinear increase in the internal stress between the matrix and the AHS component.

The data on the susceptibility of T_1 and T_2 to hydrostatic pressure in bulk AHS and some nanocomposites are summarized in Table 2. Due to opposite sign of baric coefficients ($dT_1/dp > 0$ and $dT_2/dp < 0$) the temperature interval of ferroelectric Pc phase existence is expanding under external pressure.

Taking into account the uncertainty in the experimental determination of $(dT_1/dp)_{exp}$, one can assume that this value changes insignificantly with a change

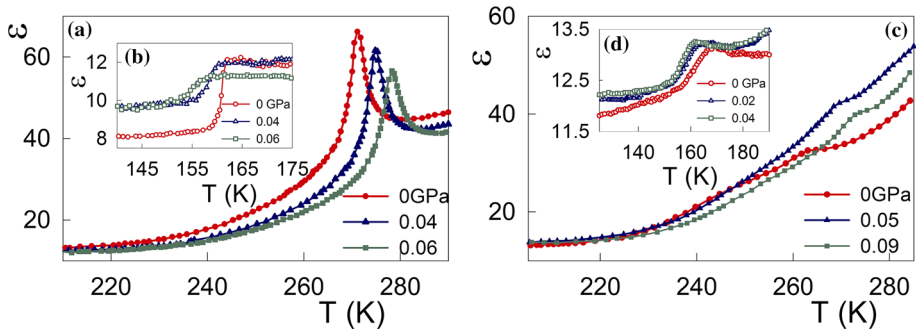

Figure 9 Temperature dependences of permittivity for **a**, **b** AHS melt and **c**, **d** AHS + PG320 measured upon heating at different pressures. Insets show behavior of ε near T_2.

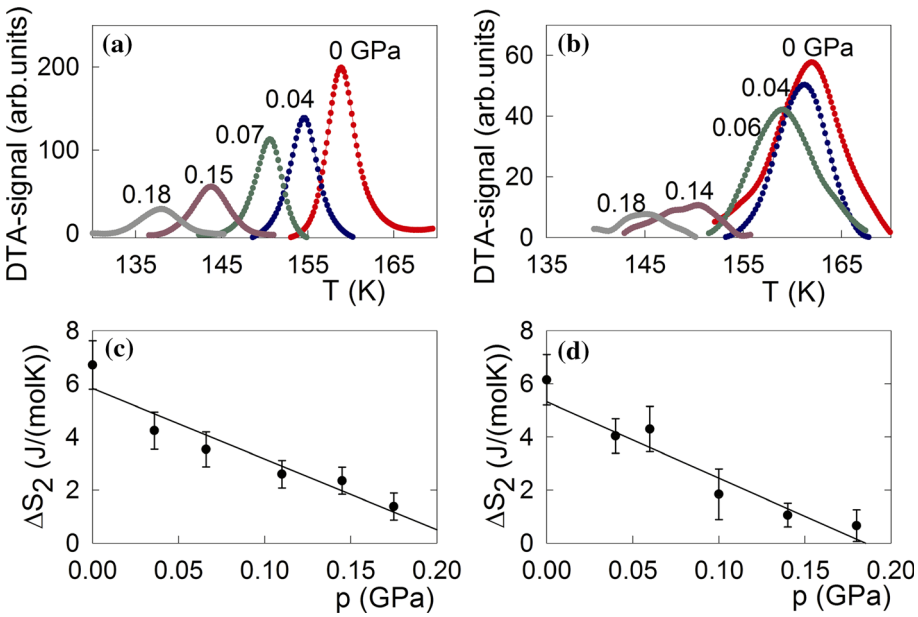

Figure 10 **a**, **b** Anomalous component of the DTA signal near T_2 at different pressures in AHS and AHS + PG320, respectively. **c**, **d** Entropy change ΔS_2 at the first-order transition in bulk AHS and AHS + PG320, respectively. The lines in (**c**) and (**d**) represent linear fits.

Table 2 Comparison of susceptibility of phase transition temperatures to hydrostatic pressure

Sample	d_{cryst} (nm)	T_1 (K)	$(dT_1/dp)_{exp}$ (K GPa^{-1})	T_2 (K)	$(dT_2/dp)_{exp}$ (K GPa^{-1})	$(dT_2/dp)_{calc}$ (K GPa^{-1})
AHS	Bulk	270.5 ± 0.2	90 ± 15	159.0 ± 0.2	− 123 ± 10	− 143 ± 20
AHS + PG160	500	268.0 ± 0.2		161.0 ± 0.2		− 98 ± 15
AHS + PG320	115	263.0 ± 0.5	115 ± 20	161.0 ± 0.2	− 88 ± 12	− 72 ± 15
AHS + PG23	70	260.0 ± 1.0		156.0 ± 0.5		− 45 ± 15
AHS + PG46	47	258.0 ± 0.5	86 ± 20	151.0 ± 0.5	− 78 ± 12	− 56 ± 15
AHS + PG5	9	251.0 ± 2.0		150.0 ± 1.0		~ (− 130)

$(dT_i/dp)_{exp}$ and $(dT_i/dp)_{calc}$ are experimental and calculated baric coefficients, respectively

of the nanoparticle size. More pronounced effect was observed in reduction of the $(dT_2/dp)_{exp}$ magnitude depending on d_{cryst}. Using the data on the entropy ΔS_2 and strain $(\Delta V/V)_{T2}$ at the first-order phase transition P-1 ↔ Pc (Fig. 6b), we have also evaluated the baric coefficient dT_2/dp for all the samples under study in the framework of the Clausius–Clapeyron equation (Table 2). It is seen that the values $|dT_2/dp|_{calc}$ are decreased except AHS + PG5, where very large baric coefficient can be due to large error in determination of the strain change $(\Delta V/V)_{T2}$.

The evaluation of the dT_1/dp baric coefficient was not carried out because of strong smeared anomalies of heat capacity and coefficient of the thermal expansion at T_1 in the nanocomposites.

There is a good agreement of the T_2 dependence on the pores size in AHS + PG observed in the present paper and in previous studies [17, 18]. However, we found a rather strong decrease in T_1 with decreasing d_{cryst} contrary to [17, 18] where this value was observed almost constant.

Let us compare the data on impact of the d_{cryst} size and external pressure on the phase transition temperatures in AHS + PG. One can suggest two mechanisms leading to the common and specific features in the behavior of T_1 and T_2. One of them is associated with a large difference in the nonanomalous thermal expansion of AHS and PG ($\alpha_{AHS} > \alpha_{PG}$) leading to the appearance of the tensile stresses in ferroelectric component. This mechanism probably plays the primary role in the samples with d_{cryst} > 100 nm. Contrary to hydrostatic pressure effect (Table 2), T_1 and T_2 in these nanocomposites were found decreased and increased, respectively, compared to bulk AHS. The value of internal pressure was evaluated using the data on T_2 in AHS and

AHS + PG160 and dT_2/dp for AHS. It was found that the increase in T_2 observed in composite (2 K) at the absence of external pressure can be generated by negative pressure of about − 0.015 GPa.

Another mechanism for changing the temperature of phase transitions in ferroelectric nanoparticles is associated with a change in the balance between the short and long interactions [42–44]. We assume that this mechanism plays a predominant role in composites with a small particle size, $d_{cryst} < 100$ nm. Indeed, both T_1 and T_2 decrease with decreasing d_{cryst}. The data presented in Table 2 support this point.

Conclusions

Heat capacity, thermal dilatation, susceptibility to hydrostatic pressure and dielectric properties of the series of the nanocomposites AHS + PG were investigated.

X-ray characterization has shown the formation of the dendrite clusters with the size exceeding the pore size in some AHS + PG like it was observed in the nanocomposites with the embedded $NaNO_2$ [12].

A small anisotropy of the linear thermal expansion of the nanocomposites is the result of statistically uniform distribution of AHS with equiprobable orientations of crystalline nanoparticles over the matrix.

The specific features of the phase transition temperatures T_1 and T_2 on d_{cryst} are related for at least two reasons: tensile stresses in the nanocomposites and a size effect. The difference in the susceptibility of T_1 and T_2 to external pressure can be due to the different mechanism of structural distortions.

A significant reduction in the entropy ΔS_2 and volume strain $(\Delta V/V)_{T2}$ at T_2 with the d_{cryst} decrease can be explained by the decrease in disorder of structural elements in the initial phase $P2_1/c$ of AHS confined in glass matrix.

Effects of external hydrostatic pressure and internal pressure associated with a decrease in d_{cryst} are similar and accompanied with: (a) a decrease in the anomalous permittivity changes at T_1 and T_2; (b) a significant reduction in the entropy and volume deformation associated with the phase transition $P\text{-}1 \leftrightarrow Pc$ in AHS and AHS + PG320.

Acknowledgements

The reported study was funded by Russian Foundation for Basic Research (RFBR) according to the Research Project No. 16-32-00092 mol_a.

Compliance with ethical standards

Conflict of interest The authors declare that they have no conflicts of interest.

References

[1] Gutina A, Antropova T, Rysiakiewicz-Pasek E, Virnik K, Feldman Yu (2003) Dielectric relaxation in porous glasses. Micropor Mesopor Mater 58:237–254

[2] Kumzerov Y, Vakhrushev S (2007) Nanostructures within porous materials. In: Nalwa HS (ed) Encyclopedia of nanoscience and nanotechnology. American Scientific Publishers, New York, pp 1–39

[3] Longo E, La Porta FA (eds) (2017) Recent advances in complex functional materials from design to application. Springer, Berlin

[4] Naberezhnov AA, Ryukhtin V, Sysoeva AA (2017) Internal structure of magnetic porous glasses and the related ferroelectric nanocomposites. Phys Solid State 59:378–384

[5] Deshmukh K, Ahamed MB, Sadasivuni KK, Ponnamma D, Deshmukh RR, Trimukhe AM, Pasha SSK, Polu AR, Al Maadeed MA-A, Chidambaram K (2017) Solution-processed white graphene-reinforced ferroelectric polymer nanocomposites with improved thermal conductivity and dielectric properties for electronic encapsulation. J Polym Res 24:27–31

[6] Komalavalli P, Banu I (2018) Enhanced room temperature multiferroic properties of nickel ferrite and lithium niobate nanocomposites. J Mater Sci: Mater Electron 29:3980–3984

[7] Ciżman A, Bednarski W, Antropova TV, Pshenko O, Rysiakiewicz-Pasek E, Waplak S, Poprawski R (2014) Structural, dielectric, thermal and electron magnetic resonance studies of magnetic porous glasses filled with ferroelectrics. Composites Part B 64:16–23

[8] Pshenko OA, Drozdova IA, Polyakova IG, Rogacki K, Ciżman A, Poprawski R, Rysiakiewicz-Pasek E, Antropova TV (2014) Ferromagnetic iron containing porous glasses. Glass Phys Chem 40:167–172

[9] Belov AN, Kislova IL, Loktev DV, Redichev EN, Stroganov AA, Solnyshkin AV (2018) Electrical characterization of poly(vinylidene fluoride-trifluoroethylene) nanocrystals embedded in porous alumina matrix. J Adv Dielectr 8:1820001

[10] Milovidova SD, Sidorkin AS, Rogazinskaya OV, Vorotnikov EV (2016) Dielectric properties of the mixed nanocomposites: triglycine sulfate–silica. Ferroelectrics 497:69–73

[11] Kinka M, Banys J, Naberezhnov A (2007) Dielectric properties of sodium nitrite confined in porous glass. Ferroelectrics 348:67–74

[12] Fokin A, Kumzerov Yu, Koroleva E, Naberezhnov A, Smirnov O, Tovar M, Vakhrushev S, Glazman M (2009) Ferroelectric phase transitions in sodium nitrite nanocomposites. J Electroceram 22:270–275

[13] Rogazinskaya OV, Milovidova SD, Sidorkin AS, Popravko NG, Bosykh MA, Enshina VS (2010) Dielectric properties of ferroelectric composites with TGS inclusions. Ferroelectrics 397:191–197

[14] Tarnavich V, Korotkov L, Karaeva O, Naberezhnov A, Rysiakiewicz-Pasek E (2010) Effect of restricted geometry on structural phase transitions in KH_2PO_4 and $NH_4H_2PO_4$ crystals. Opt Appl 40:305–309

[15] Rogazinsksya OV, Sidorkin AS, Milovidova SD, Naberezhnov AA, Matveev NN, Popravko NG, Fokin AV (2010) Ferroelectricity in nanocomposites based on porous glass with inclusions of $NaNO_2$. Bull Russ Acad Sci Phys 75:1327–1330

[16] Cizman A, Antropova T, Anfimova I, Drozdova I, Rysiakiewicz-Pasek E, Radojewska EB, Poprawski R (2013) Size driven ferroelectric–paraelectric phase transition in TGS nanocomposites. J Nanopart Res 15:1807

[17] Cizman A, Marciniszyn T, Enke D, Barascu A, Poprawski R (2013) Phase transition in NH_4HSO_4–porous glasses nanocomposites. J Nanopart Res 15:1756

[18] Baryshnikov SV, Milinskiy AYu, Charnaya EV, Bugaev AS, Samoylovich MI (2016) Dielectric studies of ferroelectric NH_4HSO_4 nanoparticles embedded into porous matrices. Ferroelectrics 493:85–92

[19] Rysiakiewicz-Pasek E, Ciżman A, Drozdova I, Polyakova I, Antropova T (2016) Synthesis, structure and properties of mixed KNO_3–$NaNO_3$ embedded into nanoporous silica glasses. Compos Part B Eng 91:291–295

[20] Kutnjak Z, Vodopivec B, Blinc R, Fokin AV, Kumzerov YA, Vakhrushev SB (2005) Calorimetric and dielectric studies of ferroelectric sodium nitrite confined in a nanoscale porous glass matrix. J Chem Phys 123:084708

[21] Rysiakiewicz-Pasek E, Poprawski R, Polanska J, Urbanowicz A, Sieradzki A (2006) Properties of porous glasses with embedded ferroelectric materials. J Non Cryst Solids 352:4309–4314

[22] Kumzerov Y, Kartenko NF, Parfen'eva LS, Smirnov IA, Fokin AV, Wlosewicz D, Misiorek H, Jezowski A (2011) Capacity and thermal conductivity of a nanocomposite chrysolite asbestos–KDP (KH_2PO_4). Phys Solid State 53:1099–1103

[23] Cizman A, Marciniszyn T, Poprawski R (2012) Pressure effect on the ferroelectric phase transition in nanosized NH_4HSO_4. J Appl Phys 112:034104

[24] San-Miguel A (2006) Nanomaterials under high-pressure. Chem Soc Rev 35:876–889

[25] Pepinsky R, Vedam K, Okaya YS, Hosino S (1958) Ammonium hydrogen sulfate: a new ferroelectric with low coercive field. Phys Rev 111:1508–1510

[26] Flerov IN, Zinenko VI, Zherebtsova LI, Iskornev IM, Blat DCh (1975) Study of phase transitions in ammonium hydrosulfate. Izvestiya AN USSR (seriya fizicheskaya) 39:752–757

[27] Swain D, Bhadram VS, Chowdhury P, Narayana C (2012) Raman and X-ray investigations of ferroelectric phase transition in NH_4HSO_4. J Phys Chem A 116:223–230

[28] Mikhaleva EA, Flerov IN, Bondarev VS, Gorev MV, Vasiliev AD, Davydova TN (2011) Phase transitions and caloric effects in ferroelectric solid solutions of ammonium and rubidium hydrosulfates. Phys Solid State 53:510–517

[29] Mikhaleva EA, Flerov IN, Kartashev AV, Gorev MV, Bogdanov EV, Bondarev VS (2017) Thermal, dielectric and barocaloric properties of NH_4HSO_4 crystallized from an aqueous solution and the melt. Solid State Sci 67:1–7

[30] Kosova DA, Emelina AL, Bykov MA (2014) Phase transitions of some sulfur-containing ammonium salts. Thermochim Acta 595:61–66

[31] Bruker AXS TOPAS V4 (2008) General profile and structure analysis software for powder diffraction data—user's manual. Bruker AXS, Karlsruhe

[32] Rysiakiewicz-Pasek E, Popravski R, Urbanowicz A, Maczka M (2005) Porous glasses with sodium nitrite impregnations. Opt Appl 35:769–774

[33] Kartashev AV, Flerov IN, Volkov NV, Sablina KA (2008) Adiabatic calorimetric study of the intense magnetocaloric effect and the heat capacity of $(La_{0.4}Eu_{0.6})_{0.7}Pb_{0.3}MnO_3$. Phys Solid State 50:2115–2120

[34] Shimizu H, Abe N, Yasuda N, Fujimoto S, Sawada S, Shiroishi Y (1979) Differential thermal analysis using a Ge–Ag thermocouple under hydrostatic pressure: phase behavior of $\{N(CH_3)_4\}_2MnCl_4$. Jpn J Appl Phys 18:857–858

[35] Iskornev IM, Flerov IN (1978) Thermal expansion of ferroelectric crystals of the ammonium hydrosulfate family. Fizika Tverdogo Tela 20:2649–2653

[36] Lines ME, Glass AM (1979) Principles and applications of ferroelectrics and related materials (international series of monographs on physics). Oxford University Press, Oxford

[37] Flerov IN, Mikhaleva EA (2008) Electrocaloric effect and anomalous conductivity of the ferroelectric NH_4HSO_4. Phys Solid State 50:478–484

[38] Polandov IN, Mylov VP, Strukov BA (1969) About p–T phase diagram of ferroelectric crystal NH_4HSO_4. Sov Phys Solid State 10:1754–1756

[39] Miller R, Blinc R, Brenman M, Waugh JS (1962) Nuclear spin-lattice relaxation in some ferroelectric ammonium salts. Phys Rev 126:528–532

[40] Nelmes RJ (1971) An X-ray diffraction determination of the crystal structure of ammonium hydrosulfate above the ferroelectric transition. Acta Crystallogr B 27:272–281

[41] Nelmes RJ (1972) The structure of ammonium hydrogen sulfate in its ferroelectric phase and the ferroelectric transition. Ferroelectrics 4:133–140

[42] Kretschmar R, Binder K (1979) Surface effects on phase transitions in ferroelectrics and dipolar magnets. Phys Rev B 20:1065–1076

[43] Tilley DR, Zeks B (1984) Landau theory of phase transitions in thick films. Solid State Commun 49:823–828

[44] Ishikawa K, Yoshikawa K, Okada N (1988) Size effect on the ferroelectric phase transition in $PbTiO_3$ ultrafine particles. Phys Rev B 37:5852–5855